Journal of Computational Physics 423 (2020) 109782

Contents lists available at ScienceDirect

Journal of Computational Physics

www.elsevier.com/locate/jcp

A novel second-order linear scheme for the Cahn-Hilliard-Navier-Stokes equations

Lizhen Chen [a], Jia Zhao [b,*]

[a] Beijing Computational Science Research Center, Beijing, PR China
[b] Department of Mathematics & Statistics, Utah State University, Logan, UT, USA

ARTICLE INFO

Article history:
Received 14 May 2020
Received in revised form 12 July 2020
Accepted 12 August 2020
Available online 25 August 2020

Keywords:
Phase field
Linear scheme
Cahn-Hilliard equation
Navier-Stokes equation
Energy stable

ABSTRACT

In this paper, we consider the Cahn-Hilliard equation coupled with the incompressible Navier-Stokes equation, usually known as the Cahn-Hilliard-Navier-Stokes (CHNS) system. The CHNS system has been widely embraced to investigate the dynamics of a binary fluid mixture. By utilizing the modified leap-frog time-marching method, we propose a novel numerical algorithm for solving the CHNS system in an efficient and accurate manner. This newly proposed scheme has several advantages. First of all, the proposed scheme is linear in time and space, such that only a linear algebraic system needs to be solved at each time-marching step, making it extremely efficient. Also, the existence and uniqueness of numerical solutions are guaranteed for any time step size. In addition, the scheme is unconditionally energy stable with second-order accuracy in time and spectral accuracy in space, such that relatively large temporal and spatial mesh sizes can be used to obtain reliable numerical solutions. The rigorous proofs for the unconditional energy stable property and solution existence and uniqueness are given. Furthermore, we present several numerical examples to test the proposed numerical algorithm and illustrate its accuracy and efficiency. The differences of coarsening dynamics between the Cahn-Hilliard equation and the Cahn-Hilliard-Navier-Stokes equations have been investigated as well.

1. Introduction

Interfacial dynamic problems have been intensively studied in the past decades. Among many powerful modeling and numerical tools, the hydrodynamic phase-field approach attracts the most attention, mainly due to its simplicity of formulation, and transparent relations of its model parameters to the physical properties. Also, the hydrodynamics phase-field models are usually thermodynamically consistent, i.e., the solutions obey the thermodynamics laws, making them physically sound. In particular, one intensively investigated example is the coupled system of the Cahn-Hilliard equation and incompressible Navier-Stokes equation, which has been used to study the dynamics of the binary fluid mixture. The Cahn-Hilliard-Navier-Stokes (CHNS) system is also the main focus of this paper.

Consider a domain Ω with smooth boundaries $\partial\Omega$. We use $\frac{1+\phi}{2}$ to denote the volume fraction of one component in the binary fluid mixture, such that $\frac{1-\phi}{2}$ represents the volume fraction of the other component, with $\phi \in [-1, 1]$. In this paper,

* Corresponding author.
E-mail addresses: lzchen@csrc.ac.cn (L. Chen), jia.zhao@usu.edu (J. Zhao).

https://doi.org/10.1016/j.jcp.2020.109782
0021-9991/

we assume both components have the same density ρ, and the binary fluid mixture is in-compressible. Interested readers can refer to [1,22,27,32,33,38] on the hydrodynamic phase field models for quasi-compressible or compressible binary fluids. We further denote the mass-averaged velocity as $\mathbf{u}$, and the pressure as p. Then the governing Cahn-Hilliard-Navier-Stokes (CHNS) system reads as follows.

$$\begin{cases} \partial_t \phi + \nabla \cdot (\mathbf{u}\phi) = M\Delta\mu, \\ \rho(\partial_t \mathbf{u} + \mathbf{u}\cdot\nabla\mathbf{u}) = -\nabla p + \eta\Delta\mathbf{u} - \phi\nabla\mu, \\ \nabla\cdot\mathbf{u} = 0, \end{cases} \tag{1.1}$$

with either periodic boundary conditions or the physical boundary conditions

$$\mathbf{u}|_{\partial\Omega} = 0, \quad \nabla\phi\cdot\mathbf{n}|_{\partial\Omega} = 0, \quad \nabla\mu\cdot\mathbf{n}|_{\partial\Omega} = 0. \tag{1.2}$$

Here $\eta > 0$ is the viscosity parameter, $M \geq 0$ is the mobility, and $\mu := \frac{\delta E}{\delta \phi}$ is called the chemical potential, with E the total energy of the binary fluid mixture. To close the system, we need to specify the expression of the total energy E of the system (1.1), which usually consistent two parts: the kinetic energy E_{NS} and the free energy E_{CH}, shown as below

$$E = E_{CH} + E_{NS}. \tag{1.3}$$

The kinetic energy is given as

$$E_{NS} = \int_\Omega \frac{\rho}{2}|\mathbf{v}|^2 d\mathbf{x}. \tag{1.4}$$

The free energy usually depends on the physical properties of the binary fluid mixture. For two immiscible binary viscous fluid mixtures, the free energy could be proposed as

$$E_{CH} = \gamma \int_\Omega \frac{\varepsilon}{2}|\nabla\phi|^2 + \frac{1}{4\varepsilon}(\phi^2-1)^2 d\mathbf{x}, \tag{1.5}$$

where ε relates to the interfacial thickness, and γ is the surface tension parameter.

It is known that the total energy E of the CHNS system (1.1) is non-increasing in time, and a system with such property is known as a dissipative system. We remark that the CHNS system in (1.1) has assumed the temperature is constant, which is also usually known as isothermal dissipative system. For a non-isothermal situation, the transport equation of temperature or the internal energy shall be added. Also, when the two fluid components have different densities, the incompressible Navier-Stokes equation shall be replaced/updated, as well. In this paper, we only focus on the iso-thermal and incompressible CHNS system.

To design accurate, efficient, and stable numerical algorithms for the CHNS system have been an active field for decades. Mainly, there are several difficulties/concerns: how to deal with the nonlinear terms in the chemical potential, how to deal with the coupling between the phase variable ϕ and hydrodynamic variable $\mathbf{v}$, i.e., the coupling between the Cahn-Hilliard equation and the incompressible Navier-Stokes equation, and how to guarantee the incompressible property for the numerical solution of the velocity field. In addition, given that the CHNS system is dissipative, i.e., it satisfies an energy dissipation law, one golden principle for the algorithm designs are that the algorithm shall guarantee the numerical solutions would also satisfy the energy dissipation laws in the discrete levels. Such types of numerical schemes are usually named energy-stable schemes. And if an algorithm has such property and it does not depend on the time step, the algorithm is then known as unconditionally energy stable scheme [18]. Otherwise, if the numerical schemes are not energy stable, the numerical solutions will break the hidden dissipative physics the CHNS system represents.

There are many existing results in the literature on addressing these difficulties. Here are some relevant work that attracts our attention [2,3,9,11–13,15–17,19,21,23,26,28,29,31,33,35,36,39,45,47]. Interested readers are recommended to read these papers and the references therein. In particular, to deal with the nonlinearity in the Cahn-Hilliard equation (for the chemical potential), there are many deeply discussed approaches, including the stabilized approach, convex splitting approach, invariant energy quadratization (IEQ) approach, scalar auxiliary variable (SAV) approach, Taylor expansion approach, discrete energy variation approach, and many others [8,28,40,41,43,44,46,49]. In order to decouple the incompressible Navier-Stokes equation and the Cahn-Hilliard equation, one can use the operator splitting technique [30,39,42,48]. However, we emphasize that such decoupling is restricted to the first-order accuracy in time, due to the splitting error. How to design a second-order decoupling scheme for the CHNS system is still an open question.

In addition, we want to point out several relevant numerical work of the CHNS system. In [36], the authors are the pioneers (to our best knowledge) to propose a second-order accurate time marching scheme for the CHNS system. They use the convex splitting idea for discretizing the nonlinear terms in the chemical potential, and use the pressure projection method to decouple the flow field $\mathbf{u}$ and pressure p. The Newton iteration method has to be applied in each time marching step, given the Navier-Stokes equation is still coupled with the Cahn-Hilliard equation, and the scheme is nonlinear. This significantly increases the computational cost. To avoid the nonlinear iteration, the authors in [23] propose to discretize

the nonlinear term in the chemical potential with the IEQ approach, such that each time step, only a linear system is required to be solved. In [35], the authors propose a Crank-Nicolson-leapfrog linear scheme based on the IEQ approach. Furthermore, the SAV approach [41] could also be used to arrive at more efficient linear schemes for the CHNS system. However, as a drawback, the IEQ and SAV approach modified the free energy with new auxiliary variables, such that the direct connections between the modified energy and the original energy in the discrete level are not clear anymore. In the meanwhile, numerical algorithms for solving the quasi-incompressible phase-field hydrodynamic models have also been developed [25,33,34].

In this paper, by embracing the modified leap-frog time-marching approach [7], we propose a novel numerical algorithm to address some deficiency of the existing numerical schemes for the CHNS system mentioned above. This newly proposed scheme has several merits to make it stand out. First of all, unlike the IEQ approach [49] or SAV approach [41], as well their generalized extensions, for which the expression of the energy is modified with the auxiliary variables, the newly proposed schemes satisfy an energy dissipation law that is expressed by the original variables. Next, unlike the convex-splitting nonlinear schemes [18,36], for which nonlinear iterative Newton's method has to be applied, the newly proposed scheme is fully linear such that only a linear system shall be solved at each time marching step, which is more computationally efficient. As a by-product, the solution's existence and uniqueness could be easily verified. Furthermore, we emphasize that the proposed numerical techniques in this paper could be efficiently utilized to investigate other hydrodynamics phase-field models for multiphase fluids, quasi-incompressible fluids, and complex fluids. These general applications will be investigated in our later research projects.

The rest of the paper is organized as follows. In Section 2, we revisit the Cahn-Hilliard-Navier-Stokes (CHNS) system, and its properties of mass conservation and energy dissipation. Then we propose a second-order temporal discretization. The energy stability is also shown for the temporal semi-discrete scheme. Then we discretize the space using the pseudo-spectral method. The energy stability, the solution existence and uniqueness, and the mass conservation property for the full-discrete scheme are proved. In Section 3, we implement the proposed scheme and show several numerical examples to demonstrate the efficiency and accuracy of the proposed scheme. In the end, we give a brief conclusion.

2. Numerical schemes

For simplicity of notations, we assume periodic boundary conditions for the CHNS system in the rest of this paper, otherwise specified. Note that all the following results also apply for the CHNS system with physical boundary conditions in (1.2).

First of all, we introduce the following notations. For any $f, g \in L^2(\Omega)$, we denote the L^2 inner product and the induced norm as below

$$(f, g) = \int_\Omega f g d\mathbf{x}, \quad \|f\| = \sqrt{(f, f)}. \tag{2.1}$$

It could be verified that the CHNS system of (1.1) satisfies the following two properties: 1) it preserves the total mass of each fluid components, i.e.

$$\frac{d}{dt}\int_\Omega \frac{1+\phi}{2} d\mathbf{x} = 0, \quad \frac{d}{dt}\int_\Omega \frac{1-\phi}{2} d\mathbf{x} = 0, \tag{2.2}$$

and 2) it follows an energy dissipation law as

$$\frac{d}{dt}E = -M\|\nabla\mu\|^2 - \eta\|\nabla\mathbf{u}\|^2, \tag{2.3}$$

with E defined in (1.3), and $\mu = \frac{\delta E}{\delta \phi}$ the chemical potential. In this paper, we are interested in designing numerical algorithms that can preserve the mass, and guarantee the energy dissipation for the numerical solutions. In the meanwhile, the designed numerical algorithm shall be easy to be implemented and efficient to be solved.

To design the time-marching numerical scheme, we denote the skew-symmetric operator B [36] as

$$B(\mathbf{v}, \mathbf{u}) = (\mathbf{v}\cdot\nabla)\mathbf{u} + \frac{1}{2}(\nabla\cdot\mathbf{v})\mathbf{u}, \tag{2.4}$$

and we rewrite the CHNS system in (1.1) as

$$\begin{cases} \partial_t\phi + \nabla\cdot(\mathbf{u}\phi) = M\Delta\mu, \\ \mu = -\varepsilon\gamma\Delta\phi + \frac{\gamma}{\varepsilon}(\phi^3 - \phi), \\ \rho(\partial_t\mathbf{u} + B(\mathbf{u}, \mathbf{u})) = -\nabla p + \eta\Delta\mathbf{u} - \phi\nabla\mu, \\ \nabla\cdot\mathbf{u} = 0, \end{cases} \tag{2.5}$$

with either periodic boundary conditions or the physical boundary conditions

$$\mathbf{u}|_{\partial\Omega} = 0, \quad \nabla\phi \cdot \mathbf{n}|_{\partial\Omega} = 0, \quad \nabla\mu \cdot \mathbf{n}|_{\partial\Omega} = 0. \tag{2.6}$$

We note equation (2.5) is equivalent with (1.1) due to the incompressibility condition $\nabla \cdot \mathbf{u} = 0$. We will focus on (2.5) in the rest of this paper.

2.1. Temporal discretization

Consider the CHNS system in (2.5) for the time domain $[0, T]$. We discretize it with a uniform time step, $0 = t_0 < t_1 < t_2 < \ldots < t_N = T$, with $t_n = \frac{n}{N}T$, and we denote the numerical solutions at t_n as $(\mathbf{u}^n, \phi^n, p^n)$, $0 \le n \le N$. Then, a second-order linear, semi-discrete numerical scheme in time is proposed below.

Scheme 2.1. *After we obtain $(\mathbf{u}^{n-1}, \phi^{n-1}, p^{n-1})$ and $(\mathbf{u}^n, \phi^n, p^n)$, we can obtain $(\mathbf{u}^{n+1}, \phi^{n+1}, p^{n+1})$, $\forall n \ge 1$, via the following two step schemes:*

- *Step 1, solve $(\phi^{n+1}, \hat{\mathbf{u}}^{n+1})$ via the following scheme*

$$\frac{1}{2\delta t}(\phi^{n+1} - \phi^{n-1}) + \nabla \cdot (\phi^n \frac{\hat{\mathbf{u}}^{n+1} + \mathbf{u}^{n-1}}{2}) = M\Delta\mu^n, \tag{2.7}$$

$$\mu^n = -\gamma\varepsilon\Delta\frac{\phi^{n+1} + \phi^{n-1}}{2} + \frac{\gamma}{\varepsilon}(\phi^n)^2\frac{\phi^{n+1} + \phi^{n-1}}{2} - \frac{\gamma}{\varepsilon}\phi^n + C(\phi^{n+1} - 2\phi^n + \phi^{n-1}), \tag{2.8}$$

$$\frac{\rho}{2\delta t}(\hat{\mathbf{u}}^{n+1} - \mathbf{u}^{n-1}) + \rho B(\mathbf{u}^n, \frac{\hat{\mathbf{u}}^{n+1} + \mathbf{u}^{n-1}}{2}) = -\nabla p^{n-1} + \eta\Delta\frac{\hat{\mathbf{u}}^{n+1} + \mathbf{u}^{n-1}}{2} - \phi^n\nabla\mu^n, \tag{2.9}$$

with $C > 0$ the stabilization parameter, and either periodic boundary conditions or the following physical boundary conditions

$$\hat{\mathbf{u}}^{n+1}|_{\partial\Omega} = 0, \quad \nabla\phi^{n+1} \cdot \mathbf{n}|_{\partial\Omega} = 0, \quad \nabla\mu^n \cdot \mathbf{n}|_{\partial\Omega} = 0. \tag{2.10}$$

- *Step 2, solve $(\mathbf{u}^{n+1}, p^{n+1})$ via the following scheme*

$$\frac{\rho}{2\delta t}(\mathbf{u}^{n+1} - \hat{\mathbf{u}}^{n+1}) + \frac{1}{2}\nabla(p^{n+1} - p^{n-1}) = 0, \tag{2.11}$$

$$\nabla \cdot \mathbf{u}^{n+1} = 0. \tag{2.12}$$

Remark 2.1. We note that $\hat{\mathbf{u}}^{n+1}$ is an intermediate velocity variable, and in Step 2, the procedure of solving $\mathbf{u}^{n+1}$ and p^{n+1} could be decoupled. Mainly if we take divergence operation on both sides of equation (2.11), we can solve p^{n+1} via

$$-\Delta p^{n+1} = -\Delta p^{n-1} - \frac{\rho}{\delta t}\nabla \cdot \hat{\mathbf{u}}^{n+1}. \tag{2.13}$$

Then we can update $\mathbf{u}^{n+1}$ via

$$\mathbf{u}^{n+1} = -\frac{\delta t}{\rho}\nabla(p^{n+1} - p^{n-1}) + \hat{\mathbf{u}}^{n+1}. \tag{2.14}$$

Remark 2.2. In literature, the leap-frog numerical technique is usually used for hyperbolic systems, but not parabolic systems like the Cahn-Hilliard equation, due to stability issues. In this paper, we introduce a key correction by using three temporal steps to discretize the nonlinear term in the Cahn-Hilliard equation. This special treatment is critical in the energy-stability analysis for the numerical scheme.

Remark 2.3. Given the initial condition $\mathbf{u}^0, \phi^0, p^0$, we obtain $\mathbf{u}^1, \phi^1, p^1$ via a first order energy-stable time marching scheme with much smaller time steps, such that $\mathbf{u}^1, \phi^1, p^1$ is second-order accurate in term of δt.

Theorem 2.1. *The semi-discrete Scheme 2.1 is unconditionally energy stable. And the discrete energy law reads as*

$$E^{n+1,n} - E^{n,n-1} = -\delta t M(\nabla\mu^n, \nabla\mu^n) - \delta t\|\sqrt{\eta}\nabla\frac{\hat{\mathbf{u}}^{n+1} + \mathbf{u}^{n-1}}{2}\|^2, \tag{2.15}$$

where

$$
\begin{aligned}
E^{n+1,n} &= \frac{\gamma\varepsilon}{4}(\|\nabla\phi^{n+1}\|^2+\|\nabla\phi^{n}\|^2)+(\frac{\gamma}{4\varepsilon}(\phi^{n+1}\phi^{n}-1)^2,1)+\frac{C}{2}\|\phi^{n+1}-\phi^{n}\|^2\\
&\quad+\frac{\rho}{4}(\|\mathbf{u}^{n+1}\|^2+\|\mathbf{u}^{n}\|^2)+\frac{\delta t^2}{4\rho}(\|\nabla p^{n+1}\|^2+\|\nabla p^{n}\|^2),\\
E^{n,n-1} &= \frac{\gamma\varepsilon}{4}(\|\nabla\phi^{n}\|^2+\|\nabla\phi^{n-1}\|^2)+(\frac{\gamma}{4\varepsilon}(\phi^{n}\phi^{n-1}-1)^2,1)+\frac{C}{2}\|\phi^{n}-\phi^{n-1}\|^2\\
&\quad+\frac{\rho}{4}(\|\mathbf{u}^{n}\|^2+\|\mathbf{u}^{n-1}\|^2)+\frac{\delta t^2}{4\rho}(\|\nabla p^{n}\|^2+\|\nabla p^{n-1}\|^2).
\end{aligned}
\tag{2.16}
$$

Proof. Taking the inner product of (2.7) with $\delta t\mu^n$, we have

$$
\Big(\frac{\phi^{n+1}-\phi^{n-1}}{2},\mu^n\Big)+\delta t\Big(\mu^n,\nabla\cdot(\phi^n\frac{\hat{\mathbf{u}}^{n+1}+\mathbf{u}^{n-1}}{2})\Big)=-M\delta t(\nabla\mu^n,\nabla\mu^n).
\tag{2.17}
$$

Taking the inner product of (2.8) with $\frac{1}{2}(\phi^{n+1}-\phi^{n-1})$, we have

$$
\begin{aligned}
&\Big(\frac{\phi^{n+1}-\phi^{n-1}}{2},\mu^n\Big)=\frac{\gamma\varepsilon}{4}\Big(\|\nabla\phi^{n+1}\|^2-\|\nabla\phi^{n-1}\|^2\Big)+\frac{\gamma}{4\varepsilon}\Big((\phi^{n+1}\phi^{n})^2-(\phi^{n}\phi^{n-1})^2\\
&-2\phi^{n+1}\phi^{n}+2\phi^{n}\phi^{n-1},1\Big)+\frac{C}{2}\Big(\|\phi^{n+1}-\phi^{n}\|^2-\|\phi^{n}-\phi^{n-1}\|^2\Big).
\end{aligned}
\tag{2.18}
$$

Subtracting equation (2.18) from (2.17), we have

$$
E_{CH}^{n+1,n}-E_{CH}^{n,n-1}+\delta t\Big(\mu^n,\nabla\cdot(\phi^n\frac{\hat{\mathbf{u}}^{n+1}+\mathbf{u}^{n-1}}{2})\Big)=-M\delta t(\nabla\mu^n,\nabla\mu^n),
\tag{2.19}
$$

where $E_{CH}^{n+1,n}$ and $E_{CH}^{n,n-1}$ are defined as

$$
\begin{aligned}
E_{CH}^{n+1,n} &= \frac{\gamma\varepsilon}{4}(\|\nabla\phi^{n+1}\|^2+\|\nabla\phi^{n}\|^2)+\frac{\gamma}{4\varepsilon}((\phi^{n+1}\phi^{n}-1)^2,1)+\frac{C}{2}\|\phi^{n+1}-\phi^{n}\|^2.\\
E_{CH}^{n,n-1} &= \frac{\gamma\varepsilon}{4}(\|\nabla\phi^{n}\|^2+\|\nabla\phi^{n-1}\|^2)+\frac{\gamma}{4\varepsilon}((\phi^{n}\phi^{n-1}-1)^2,1)+\frac{C}{2}\|\phi^{n}-\phi^{n-1}\|^2.
\end{aligned}
\tag{2.20}
$$

Taking inner product of (2.9) with $\frac{\delta t}{2}(\hat{\mathbf{u}}^{n+1}+\mathbf{u}^{n-1})$, we have

$$
\begin{aligned}
\frac{\rho}{4}(\|\hat{\mathbf{u}}^{n+1}\|^2-\|\mathbf{u}^{n-1}\|^2) &= -\delta t\|\sqrt{\eta}\nabla\frac{\hat{\mathbf{u}}^{n+1}+\mathbf{u}^{n-1}}{2}\|^2-\Big(\frac{\delta t}{2}(\hat{\mathbf{u}}^{n+1}+\mathbf{u}^{n-1}),\nabla p^{n-1}\Big)\\
&\quad-\delta t\Big(\frac{\hat{\mathbf{u}}^{n+1}+\mathbf{u}^{n-1}}{2},\phi^n\nabla\mu^n\Big),
\end{aligned}
\tag{2.21}
$$

by noticing the fact

$$
\Big(\frac{\delta t}{2}(\hat{\mathbf{u}}^{n+1}+\mathbf{u}^{n-1}),B(\mathbf{u}^n,\frac{\hat{\mathbf{u}}^{n+1}+\mathbf{u}^{n-1}}{2})\Big)=0.
\tag{2.22}
$$

Taking inner product of (2.11) with $\delta t^2\nabla p^{n-1}$

$$
\rho\Big(\delta t^2\nabla p^{n-1},\frac{\mathbf{u}^{n+1}+\mathbf{u}^{n-1}-(\hat{\mathbf{u}}^{n+1}+\mathbf{u}^{n-1})}{2\delta t}\Big)-\Big(\delta t^2\nabla p^{n-1},\frac{1}{2}\nabla(p^{n+1}-p^{n-1})\Big)=0
\tag{2.23}
$$

i.e.,

$$
-\Big(\frac{\delta t}{2}(\hat{\mathbf{u}}^{n+1}+\mathbf{u}^{n-1}),\nabla p^{n-1}\Big)+\frac{\delta t^2}{4\rho}\Big(\|\nabla p^{n+1}\|^2-\|\nabla p^{n-1}\|^2-\|\nabla(p^{n+1}-p^{n-1})\|^2\Big)=0.
\tag{2.24}
$$

Taking the inner product of (2.11) with $\delta t\mathbf{u}^{n+1}$

$$
\frac{\rho}{4}(\|\mathbf{u}^{n+1}\|^2-\|\hat{\mathbf{u}}^{n+1}\|^2+\|\mathbf{u}^{n+1}-\hat{\mathbf{u}}^{n+1}\|^2)=0.
\tag{2.25}
$$

From (2.11), we know

$$
\frac{\delta t^2}{4\rho}\|\nabla p^{n+1}-\nabla p^{n-1}\|^2-\frac{\rho}{4}\|\mathbf{u}^{n+1}-\hat{\mathbf{u}}^{n+1}\|^2=0.
\tag{2.26}
$$

Adding these equations (2.21), (2.24), (2.25) and (2.26) together, we can easily see

$$E_{NS}^{n+1,n} - E_{NS}^{n,n-1} + \delta t\Big(\frac{\hat{\mathbf{u}}^{n+1}+\mathbf{u}^{n-1}}{2}, \phi^n\nabla\mu^n\Big) = -\delta t\|\sqrt{\eta}\nabla\frac{\hat{\mathbf{u}}^{n+1}+\mathbf{u}^{n-1}}{2}\|^2, \tag{2.27}$$

where

$$\begin{aligned} E_{NS}^{n+1,n} &= \frac{\rho}{4}(\|\mathbf{u}^{n+1}\|^2 + \|\mathbf{u}^n\|^2) + \frac{\delta t^2}{4\rho}(\|\nabla p^{n+1}\|^2 + \|\nabla p^n\|^2), \\ E_{NS}^{n,n-1} &= \frac{\rho}{4}(\|\mathbf{u}^{n}\|^2 + \|\mathbf{u}^{n-1}\|^2) + \frac{\delta t^2}{4\rho}(\|\nabla p^{n}\|^2 + \|\nabla p^{n-1}\|^2). \end{aligned} \tag{2.28}$$

Notice the fact

$$\delta t\Big(\mu^n, \nabla\cdot(\phi^n\frac{\hat{\mathbf{u}}^{n+1}+\mathbf{u}^{n-1}}{2})\Big) + \delta t\Big(\frac{\hat{\mathbf{u}}^{n+1}+\mathbf{u}^{n-1}}{2}, \phi^n\nabla\mu^n\Big) = 0, \tag{2.29}$$

for periodic boundary condition or the physical boundary condition in (2.10).

Adding the equations (2.19), (2.27), and (2.29), we finally get

$$E^{n+1,n} - E^{n,n-1} = -M\delta t(\nabla\mu^n, \nabla\mu^n) - \delta t\|\sqrt{\eta}\nabla\frac{\hat{\mathbf{u}}^{n+1}+\mathbf{u}^{n-1}}{2}\|^2, \tag{2.30}$$

where $E^{n+1,n} = E_{CH}^{n+1,n} + E_{NS}^{n+1,n}$ and $E^{n,n-1} = E_{CH}^{n,n-1} + E_{NS}^{n,n-1}$. This completes the proof. □

Remark 2.4. In literature, there are quite a few results on the convergence analysis for the phase-field hydrodynamics models, including Cahn-Hilliard-Navier-Stokes equations, Cahn-Hilliard-Hele-Shaw equations, Cahn-Hilliard-Stokes equations. And both the first-order and second-order (in time) convergence estimates have been reported. Convergence analysis is out of research scope in this paper, interested readers are encouraged to read [5,6,10,14,37] and the references therein.

2.2. Spatial discretization

In this paper, we consider the periodic boundary conditions, so it is natural to employ the Fourier pseudo-spectral method. Here we consider a two-dimensional domain for simplicity. Note that an extension of the following results to a three-dimensional domain is trivial.

Denote the spatial domain $\Omega = [0, L_x]\times[0, L_y]$, with L_x and L_y the lengths in each direction. We discretize Ω with uniformly partitioned meshes with mesh sizes $h_x = L_x/N_x$ and $h_y = L_y/N_y$, where N_x, N_y are two positive even integers. Therefore, we have the discrete domain

$$\Omega_h = \big\{(x_i, y_j)|x_i = ih_x, y_j = jh_y, 0\le i\le N_x-1, 0\le j\le N_y-1\big\}. \tag{2.31}$$

We further introduce the space of grid functions on Ω_h, denoted as

$$V_h = \big\{u|u = \{u_{ij}|(x_i, y_j)\in\Omega_h, 0\le i\le N_x-1, 0\le j\le N_y-1\}\big\}. \tag{2.32}$$

For any two grid functions $F\in V_h, G\in V_h$, we define the discrete inner product and induced l_2 norm as follows

$$(F, G)_h = \sum_{i=0}^{N_x-1}\sum_{j=0}^{N_y-1} F_{ij}G_{ij}h_xh_y, \quad \|F\|_h = \sqrt{(F, F)_h}. \tag{2.33}$$

Following the notations in our previous work [7], we define discrete gradient operator ∇_h and the discrete Laplace operator Δ_h, and to distinguish with the semi-discrete solution ϕ^n, p^n, $\mathbf{u}^n$, $n\ge 0$ we denote the full discrete solution with an subscript, as $\phi_N^n\in V_h$, $p_N^n\in V_h$ and $\mathbf{u}_N^n\in(V_h)^2$, respectively.

Then the fully discrete numerical scheme is proposed as below.

Scheme 2.2. *After we obtain $\phi_N^{n-1}, \phi_N^n\in V_h, \mathbf{u}_N^{n-1}, \mathbf{u}_N^n\in(V_h)^2$, and $p_N^{n-1}, p_N^n\in V_h$, we update $(\phi_N^{n+1}, \mathbf{u}_N^{n+1}, p_N^{n+1})\in(V_h, (V_h)^2, V_h)$, with $n\ge 1$, via two steps.*

- *Step 1, solve ϕ_N^{n+1} and $\hat{\mathbf{u}}_N^{n+1}$ via the following scheme*

$$\frac{1}{2\delta t}(\phi_N^{n+1} - \phi_N^{n-1}) + \nabla_h\cdot(\phi_N^n\frac{\hat{\mathbf{u}}_N^{n+1}+\mathbf{u}_N^{n-1}}{2}) = M\Delta_h\mu_N^n, \tag{2.34}$$

$$\mu_N^n = -\gamma\varepsilon\Delta_h\frac{\phi_N^{n+1}+\phi_N^{n-1}}{2} + \frac{\gamma}{\varepsilon}(\phi_N^n)^2\frac{\phi_N^{n+1}+\phi_N^{n-1}}{2} - \frac{\gamma}{\varepsilon}\phi_N^n + C(\phi_N^{n+1} - 2\phi_N^n + \phi_N^{n-1}), \tag{2.35}$$

$$\frac{\rho}{2\delta t}(\hat{\mathbf{u}}_N^{n+1}-\mathbf{u}_N^{n-1})+\rho B(\mathbf{u}_N^n,\frac{\hat{\mathbf{u}}_N^{n+1}+\mathbf{u}_N^{n-1}}{2})_h=-\nabla_h p_N^{n-1}+\eta\Delta_h\frac{\hat{\mathbf{u}}_N^{n+1}+\mathbf{u}_N^{n-1}}{2}-\phi_N^n\nabla_h\mu_N^n, \tag{2.36}$$

with periodic boundary conditions. Here the discrete skew-symmetric operator B is defined as

$$B(\mathbf{v}_N,\mathbf{u}_N)_h=(\mathbf{v}_N\cdot\nabla_h)\mathbf{u}_N+\frac{1}{2}(\nabla_h\cdot\mathbf{v}_N)\mathbf{u}_N. \tag{2.37}$$

- *Step 2, solve* $\mathbf{u}_N^{n+1}$ *and* p_N^{n+1} *via the following scheme*

$$\frac{\rho}{2\delta t}(\mathbf{u}_N^{n+1}-\hat{\mathbf{u}}_N^{n+1})=-\frac{1}{2}\nabla_h(p_N^{n+1}-p_N^{n-1}), \tag{2.38}$$

$$\nabla_h\cdot\mathbf{u}_N^{n+1}=0. \tag{2.39}$$

Remark 2.5. In the full discrete scheme, the steps in (2.38)-(2.39) can be further simplified, by taking a discrete divergence on both sides, and using $\nabla_h\cdot\mathbf{u}_N^{n+1}=0$. We can get p_N^{n+1} by solving

$$-\Delta_h p_N^{n+1}=-\Delta_h p_N^{n-1}-\frac{\rho}{\delta t}\nabla_h\cdot\hat{\mathbf{u}}_N^{n+1}, \tag{2.40}$$

and then we can update $\mathbf{u}_N^{n+1}$ via

$$\mathbf{u}_N^{n+1}=-\frac{\delta t}{\rho}\nabla_h(p_N^{n+1}-p_N^{n-1})+\hat{\mathbf{u}}_N^{n+1}. \tag{2.41}$$

Remark 2.6. Given the initial condition $\mathbf{u}_N^0=I_N\mathbf{u}^0,\phi_N^0=I_N\phi^0,p_N^0=I_Np^0$. Here I_N is the interpolation operator on the space of continuous functions and valued in the finite space [7], we calculate $\mathbf{u}_N^1,\phi_N^1,p_N^1$ via a first order energy-stable time marching scheme with smaller time steps, such that $\mathbf{u}_N^1,\phi_N^1,p_N^1$ is second-order accurate in term of δt.

Some theoretical results can be obtained for the full discrete Scheme 2.2.

Theorem 2.1. *The full discrete Scheme 2.2 is unconditionally energy stable. And the full discrete solutions satisfy the following energy dissipation law*

$$E_h^{n+1,n}-E_h^{n,n-1}=-\delta tM\|\nabla_h\mu_N^n\|_h^2-\delta t\|\sqrt{\eta}\nabla_h\frac{\hat{\mathbf{u}}_N^{n+1}+\mathbf{u}_N^{n-1}}{2}\|_h^2, \tag{2.42}$$

where

$$\begin{aligned}E_h^{n+1,n}&=\frac{\gamma\varepsilon}{4}(\|\nabla\phi_N^{n+1}\|_h^2+\|\nabla\phi_N^n\|^2)+\frac{\gamma}{4\varepsilon}((\phi_N^{n+1}\phi_N^n-1)^2,1)_h+\frac{C}{2}\|\phi_N^{n+1}-\phi_N^n\|_h^2\\&\quad+\frac{\rho}{4}(\|\mathbf{u}_N^{n+1}\|_h^2+\|\mathbf{u}_N^n\|_h^2)+\frac{\delta t^2}{4\rho}(\|\nabla p_N^{n+1}\|^2+\|\nabla p_N^n\|^2),\\E_h^{n,n-1}&=\frac{\gamma\varepsilon}{4}(\|\nabla\phi_N^n\|_h^2+\|\nabla\phi_N^{n-1}\|_h^2)+\frac{\gamma}{4\varepsilon}((\phi_N^n\phi_N^{n-1}-1)^2,1)_h+\frac{C}{2}\|\phi_N^n-\phi_N^{n-1}\|_h^2\\&\quad+\frac{\rho}{4}(\|\mathbf{u}_N^n\|_h^2+\|\mathbf{u}_N^{n-1}\|_h^2)+\frac{\delta t^2}{4\rho}(\|\nabla p_N^n\|_h^2+\|\nabla p_N^{n-1}\|_h^2).\end{aligned} \tag{2.43}$$

Proof. The proof is similar to that of the semi-discrete Scheme 2.1, and we thus only show the sketch. Taking the inner product of (2.34) with $\delta t\mu_N^n$, the inner product of (2.35) with $\frac{1}{2}(\phi_N^{n+1}-\phi_N^{n-1})$, and subtracting them, we will have

$$E_{CH}^{n+1,n}-E_{CH}^{n,n-1}+\delta t\Big(\mu_N^n,\nabla_h\cdot(\phi_N^n\frac{\hat{\mathbf{u}}_N^{n+1}+\mathbf{u}_N^{n-1}}{2})\Big)_h=-M\delta t\|\nabla_h\mu_N^n\|_h^2, \tag{2.44}$$

where $E_{CH}^{n+1,n}$ and $^{n,n-1}_{CH}$ are defined as

$$\begin{aligned}E_{CH}^{n+1,n}&=\frac{\gamma\varepsilon}{4}(\|\nabla_h\phi_N^{n+1}\|_h^2+\|\nabla_h\phi_N^n\|_h^2)+\frac{\gamma}{4\varepsilon}((\phi_N^{n+1}\phi_N^n-1)^2,1)_h+\frac{C}{2}\|\phi_N^{n+1}-\phi_N^n\|_h^2.\\E_{CH}^{n,n-1}&=\frac{\gamma\varepsilon}{4}(\|\nabla_h\phi_N^n\|_h^2+\|\nabla_h\phi_N^{n-1}\|_h^2)+\frac{\gamma}{4\varepsilon}((\phi_N^n\phi_N^{n-1}-1)^2,1)_h+\frac{C}{2}\|\phi_N^n-\phi_N^{n-1}\|_h^2.\end{aligned} \tag{2.45}$$

Taking the inner product of (2.36) with $\frac{\delta t}{2}(\hat{\mathbf{u}}_N^{n+1}+\mathbf{u}_N^{n-1})$, the inner product of (2.38) with $\delta t^2\nabla p_N^{n-1}$, the inner product of (2.38) with $\delta t\mathbf{u}_N^{n+1}$, the inner product of (2.38) with itself, and then adding these equations together, we can easily see

$$E_{NS}^{n+1,n} - E_{NS}^{n,n-1} + \delta t\Big(\frac{\hat{\mathbf{u}}_N^{n+1} + \mathbf{u}_N^{n-1}}{2}, \phi_N^n \nabla \mu_N^n\Big)_h = -\delta t \|\sqrt{\eta}\nabla_h \frac{\hat{\mathbf{u}}_N^{n+1} + \mathbf{u}_N^{n-1}}{2}\|_h^2, \tag{2.46}$$

where

$$\begin{aligned} E_{NS}^{n+1,n} &= \frac{\rho}{4}(\|\mathbf{u}_N^{n+1}\|_h^2 + \|\mathbf{u}_N^n\|_h^2) + \frac{\delta t^2}{4\rho}(\|\nabla_h p_N^{n+1}\|_h^2 + \|\nabla_h p_N^n\|_h^2), \\ E_{NS}^{n,n-1} &= \frac{\rho}{4}(\|\mathbf{u}_N^{n}\|_h^2 + \|\mathbf{u}_N^{n-1}\|_h^2) + \frac{\delta t^2}{4\rho}(\|\nabla_h p_N^{n}\|_h^2 + \|\nabla_h p_N^{n-1}\|_h^2). \end{aligned} \tag{2.47}$$

Notice the fact

$$\delta t\Big(\mu_N^n, \nabla_h \cdot (\phi_N^n \frac{\hat{\mathbf{u}}_N^{n+1} + \mathbf{u}_N^{n-1}}{2})\Big)_h + \delta t\Big(\frac{\hat{\mathbf{u}}_N^{n+1} + \mathbf{u}_N^{n-1}}{2}, \phi_N^n \nabla_h \mu_N^n\Big)_h = 0, \tag{2.48}$$

for periodic boundary condition. Adding the equations (2.44), (2.46), and (2.48) will complete the proof. □

Theorem 2.2. *The full discrete Scheme 2.2 is uniquely solvable, i.e. for each time marching step, there exists a unique solution* $(\phi_N^{n+1}, \mathbf{u}_N^{n+1}, p_N^{n+1}) \in (V_h, (V_h)^2, V_h)$.

Proof. We only need to show there exists a unique solution for each step of the full discrete Scheme 2.2.

For the step in (2.34)-(2.36), with a little abuse of notations, it could be written as a algebraic linear system $AX = b$, where $X = (\mu_N^n, \phi_N^{n+1}, \hat{\mathbf{u}}_N^{n+1})$ and

$$A = \begin{bmatrix} -M\Delta_h & \frac{1}{2\delta t} & \nabla_h \cdot (\frac{\phi_N^n}{2}\bullet) \\ -1 & -\frac{\varepsilon^2}{2}\Delta_h + \frac{(\phi_N^n)^2}{2} + C & 0 \\ \phi_N^n \nabla \bullet & 0 & \frac{\rho}{2\delta t} + \rho B(\mathbf{u}_N^n, \frac{\bullet}{2})_h - \frac{\eta}{2}\Delta_h \end{bmatrix}, \tag{2.49}$$

and b are the remaining (explicit) terms. To show $AX = b$ has a unique solution, we only need to show $AX = \mathbf{0}$ has only solution $X = \mathbf{0}$.

It is obvious that $X = \mathbf{0}$ is a solution to $AX = \mathbf{0}$. Next, we prove that $X = \mathbf{0}$, provided $AX = \mathbf{0}$. Denote $X = (X_1, X_2, X_3)$. As of matter of fact, if we take inner product of $Y = (2X_1, \frac{X_2}{\delta t}, X_3)$ on both sides of $AX = 0$, we will have

$$2\|\sqrt{M}\nabla_h X_1\|_h + \frac{\varepsilon^2}{2}\|\nabla_h X_2\|_h^2 + (\frac{(\phi_N^n)^2}{2} + C, X_2^2)_h + \frac{\rho}{2\delta t}\|X_3\|_h^2 + \frac{1}{2}\|\sqrt{\eta}\nabla_h X_3\|_h^2 = 0. \tag{2.50}$$

We immediately notice $\|X_3\|_h^2 = 0$, which means $X_3 = \mathbf{0}$. Given the facts $C > 0$, we have $\|X_2\|_h^2 = 0$, which means $X_2 = \mathbf{0}$. From the second equation of $AX = \mathbf{0}$, we have

$$X_1 = \frac{\varepsilon^2}{2}\Delta_h X_2 + \Big(\frac{(\phi_N^n)^2}{2} + C\Big)X_2 = \mathbf{0}. \tag{2.51}$$

Therefore, we prove that $X = \mathbf{0}$, provided $AX = \mathbf{0}$.

This indicates the step in (2.34)-(2.36) has a unique solution. It is not hard to check the step in (2.40) and the step in (2.41) has a unique solution respectively. Hence we have shown that the full discrete Scheme 2.2 has a unique solution. □

Theorem 2.3. *The full discrete Scheme 2.2 preserves the total mass of the phase variable. In other words,*

$$(\phi_N^{n+1}, 1)_h = (\phi_N^n, 1)_h, \quad \forall n \geq 0. \tag{2.52}$$

Proof. This can be easily verified if we take the discrete inner product of equation (2.34) with ϕ_N^{n+1}, and guarantee that the starting values preserve the total mass, i.e. $(\phi_N^1, 1)_h = (\phi_N^0, 1)_h$. □

3. Numerical results

In this section, we present several numerical examples of the CHNS model in a row, using the scheme (2.34)-(2.39), to demonstrate its efficiency and accuracy. For simplicity, in the rest of this section, we choose $\rho = 1$ and periodic boundary conditions on the square domain $[0, L]^2$ with L representing the length of each boundary. And we choose $N_x = N_y = N$, with N a positive integer. Also, we denote the roughness measure function $W(t)$ as follows:

$$W(t) = \sqrt{\frac{1}{|\Omega|}\int_\Omega \Big(\phi(x, y, t) - \overline{\phi}(x, y, t)\Big)^2 d\Omega}, \tag{3.1}$$

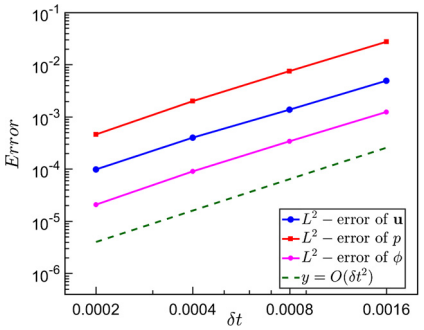

Fig. 3.1. L^2 solution errors with various time steps. This figure shows the second-order convergence rate in time of the proposed linear scheme (2.34)-(2.39) with $\eta = 0.01$, $M = 0.1$, $\gamma = 0.05$ and $\varepsilon = 0.05$.

where $\overline{\phi}(x, y, t) = \int_\Omega \phi(x, y, t) d\Omega$. Some detailed comparisons of the dynamics between the Cahn-Hilliard equation and the Cahn-Hilliard-Navier-Stokes equation are presented. And we observe that the hydrodynamics has a dramatic effect on the phase separation dynamics.

3.1. Convergence tests

First of all, we conduct a mesh-refinement test to verify the proposed scheme (2.34)-(2.39) is second-order accurate in time indeed. Consider two circular bubbles merging into a single one, starting in the middle of the domain. And we set the computational domain as $[0, 2\pi] \times [0, 2\pi]$, and fix the physical parameters $M = 0.1, \varepsilon = 0.05$, $\gamma = 0.05$, and computational parameters $N = 256, C = 2$. Then, we take the following initial conditions

$$\begin{cases} \mathbf{u}^0(x, y) = \mathbf{0}, \forall (x, y) \in \Omega, \\ \phi^0(x, y) = \begin{cases} 1, & \text{if } (x - \frac{3\pi}{4})^2 + (y - \pi)^2 \le \frac{\pi^2}{16} \text{ or } (x - \frac{5}{4}\pi)^2 + (y - \pi)^2 \le \frac{\pi^2}{16}; \\ -1, & \text{otherwise.} \end{cases} \end{cases} \tag{3.2}$$

Given the analytical solution is unknown for this problem, we take the numerical solution with $\delta t = 0.0001$ as the 'exact' solution for benchmark purpose. With the setting above, we conduct a time-step size refinement test for the full discrete scheme (2.34)-(2.39). The solution errors with various time step sizes at $t = 1$ are summarized in Fig. 3.1. We observe that the expected second order convergence rate in time for all variables is obtained as expected.

3.2. Merging bubbles

Then we investigate the evolution dynamics of two merging bubbles with the proposed scheme (2.34)-(2.39). We use the same setting as the example above. The initial condition is taken as two kissing bubbles:

$$\begin{cases} \mathbf{u}^0(x, y) = \mathbf{0}, \forall (x, y) \in \Omega, \\ \phi^0(x, y) = \tanh \dfrac{(\sqrt{(x - 0.75\pi)^2 + (y - \pi)^2} - \frac{\pi}{4}}{2\sqrt{2}\epsilon} \times \tanh \dfrac{(\sqrt{(x - 1.25\pi)^2 + (y - \pi)^2} - \frac{\pi}{4}}{2\sqrt{2}\epsilon}. \end{cases} \tag{3.3}$$

We simulate the CHNS system for the time domain $[0, 300]$ using the proposed scheme (2.34)-(2.39). Then, the time evolution of the total energy with various viscosity η is shown in Fig. 3.2(a). We observe that the energy drops dramatically at the beginning and smoothly afterward, eventually, the energies reach the steady states. We observe that the hydrodynamic equation accelerates the phase evolution dynamic in this example. Also, we observe the energy is non-increasing in time in all situations, which agrees well with our theoretical results in the previous section. The energy versus t with different δt is plotted in Fig. 3.2(b). Obviously, the dynamic with $\delta t = 0.1$ is not accurate enough. In Fig. 3.2(c), we plot the total mass, $M(t) = \int_\Omega \phi(x, y, t) d\Omega$, versus t. The mass remains a constant a least keep 10 digits the same all the time.

In Fig. 3.3, we plot the time snapshots of the phase-field profile ϕ at $t = 1$ by CHNS model with $\eta = 0.1$, $M = 0.1$, $\gamma = 0.05$. In Fig. 3.3(a), we observe that the result with $\delta t = 0.1$ is not accuracy enough in the simulation, while the result of $\delta t = 0.01$ and $\delta t = 0.001$ agree well. Thus we take $\delta t = 0.001$ in the following simulation. In Fig. 3.3(b), we see that various stability constant C does not affect the accuracy noticeably, as this term only adds a second-order error $O(\delta t^2)$. But if C is too large, the error can't be ignored. In this paper, we choose $C = 2$ if not specified otherwise. Readers can refer to [8] on discussing the optimal choices of C. In Fig. 3.3(c), the sharp interface limit is considered. And we observe the results with $\varepsilon = 0.01, 0.02$ agree well, i.e. the solutions converge to their sharp-interface limit.

In the meanwhile, the evolution history of the bubbles driven by the CH model and the CHNS model with $\eta = 1, 0.1$ are shown in Fig. 3.4. We observe they have similar dynamics, but the hydrodynamic equation does accelerate the dynamic

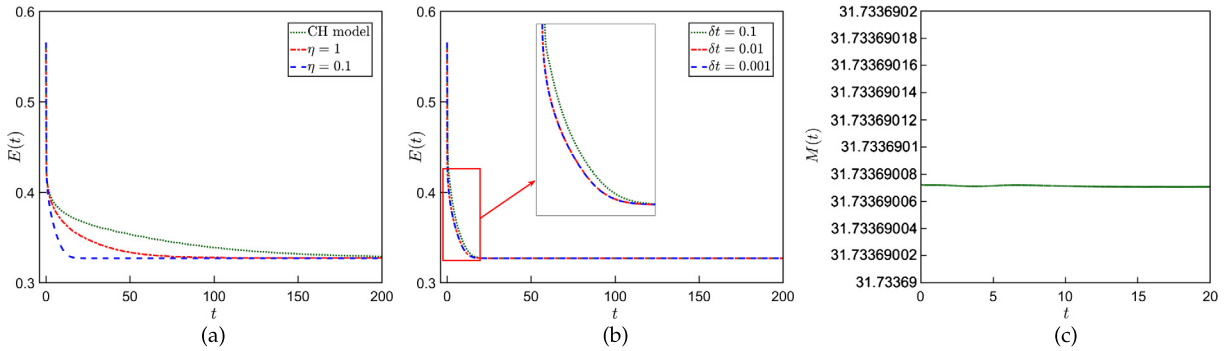

Fig. 3.2. Time evolution of the energy for the CH model and the CHNS model with various η (a), various time step δt (b) when $t \in [0, 200]$ and $M(t)$ for the CHNS model (c) when $t \in [0, 20]$.

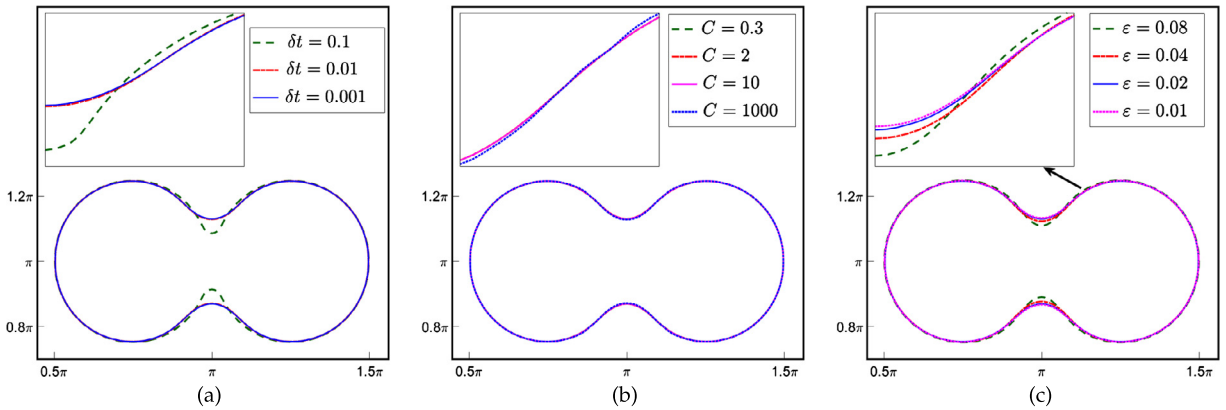

Fig. 3.3. Time snapshots of the phase field profile ϕ at $t = 1$ by the CHNS model with $\eta = 0.1$, $M = 0.1$, $\gamma = 0.05$, $\varepsilon = 0.02$. (a) takes various time steps, $\delta t = 0.1, 0.01, 0.001$; (b) takes various C values, $C = 0.3, 2.0, 10, 1000$; (c) takes various interfacial thickness, $\varepsilon = 0.08, 0.04, 0.02, 0.01$.

slowly. Also the profiles of vector $\mathbf{u}$ and the profile of pressure p at different time are presented in Fig. 3.5. We observe that the velocity vector field of CHNS model lead to vortexes around the bubbles.

In order to compare the efficiency of our method, we also compare it with the second-order IEQ scheme [24]. In Fig. 3.6 we present the energy decay for the CHNS model when $t \in [0, 50]$ with $\eta = 0.1$, $M = 0.1$, $\gamma = 0.05$ and $\varepsilon = 0.05$. We observe that the energy decay agrees well by the two schemes when δt is small, while error will increase when increasing δt. In this example, the newly proposed scheme demonstrates compatible accuracy with the IEQ scheme.

3.3. Coarsening dynamics

In the next example, we perform numerical simulations of coarsening dynamics in the computational domain $[0, 2\pi] \times [0, 2\pi]$. The initial conditions are given as below

$$\begin{cases} \mathbf{u}^0(x, y) = \mathbf{0}, \forall (x, y) \in \Omega, \\ \phi^0(x, y) = rand(-0.001, 0.001), \quad \forall (x, y) \in \Omega, \end{cases} \tag{3.4}$$

where for each point, $rand(-0.001, 0.001)$ generates a random state varying from -0.001 to 0.001. We fix the following physical parameters $M = 0.02$, $\gamma = 0.05$, $\varepsilon = 0.05$ and computational parameters $\delta t = 0.001$, $N = 256$.

As shown in Fig. 3.7(a), we observe the energy of the Cahn-Hilliard equation with constant mobility parameter decreases as $O(t^{-\frac{1}{3}})$. And the energy decreases as $O(t^{-1})$ for CHNS is also observed. All of these agree well with existing reports in literature [4]. To further investigate how the hydrodynamics would affect the coarsening dynamics, we solve the CHNS equation with various viscosities. Their energy evolution and roughness are summarized in Fig. 3.7. We observe that the hydrodynamics facilitates the coarsening dramatically. At the initial time period, the energy decays follow a much faster power law, and at later times, the energy decays with a similar power law as the CH equation alone. In other words, the hydrodynamics has a dramatic effect on the coarsening dynamics when the phase-field profile has a fine-scale.

In addition, to have a better visualization of the different dynamics produced by the CH equation and the CHNS equation, we present the phase-field profiles at various time slots in Fig. 3.8, with snapshots are taken at $t = 5, 25, 50, 100, 200$, respectively. We observe that the hydrodynamics tremendously influence the coarsening dynamics, i.e., the evolution of the

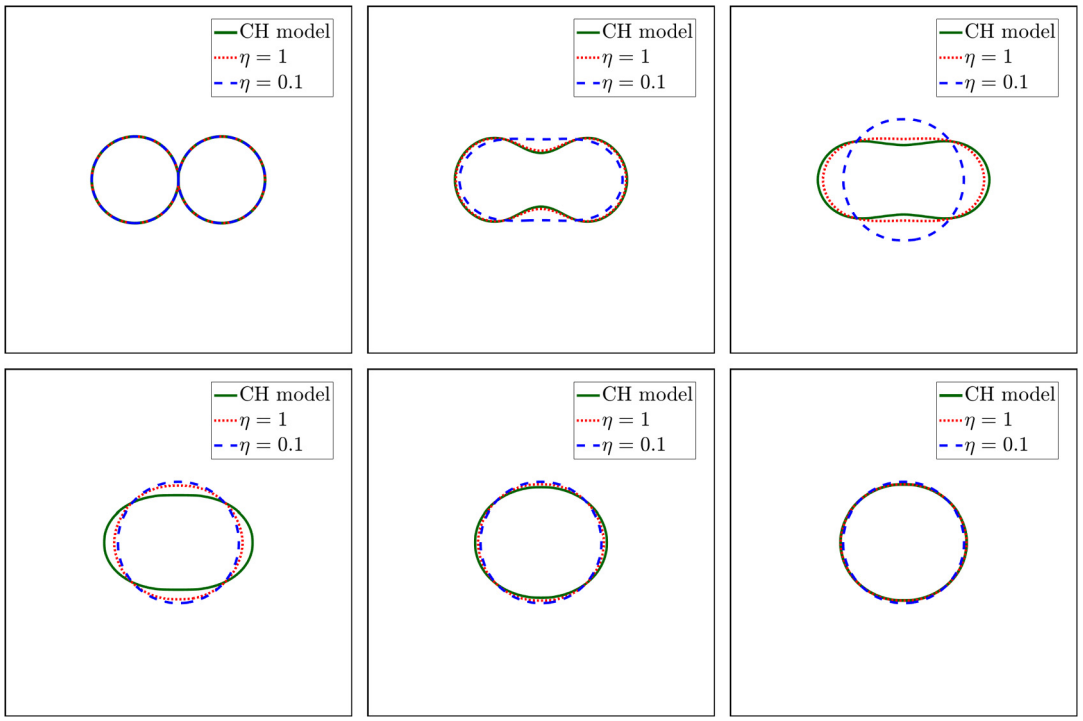

Fig. 3.4. Time snapshots of the phase field profile ϕ during coarsening dynamics. The dynamics is driven by the CH model with $M = 0.1$, $\gamma = 0.05$ and $\varepsilon = 0.02$, and the dynamics driven by the CHNS model with $\eta = 1,\ 0.1$, $M = 0.1$, $\gamma = 0.05$ and $\varepsilon = 0.02$. In both cases, the profiles of ϕ at different time slots $t = 0, 5, 20, 100, 200, 300$ are presented.

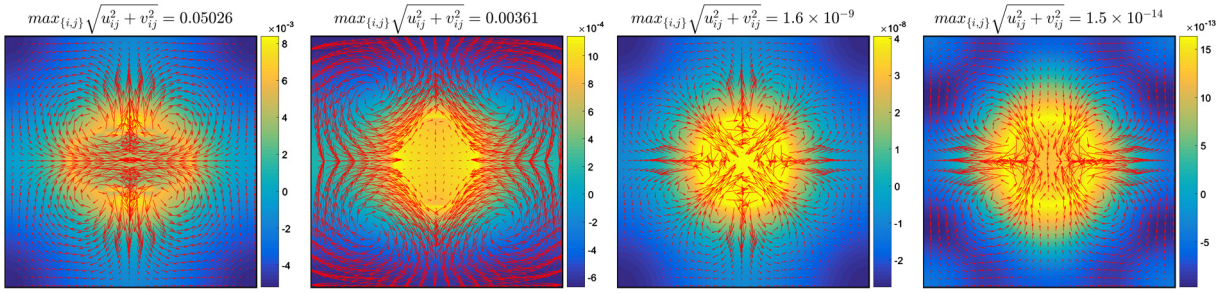

Fig. 3.5. Time snapshots of coarsening dynamics driven by the CHNS model with $\eta = 0.1$, $M = 0.1$, $\gamma = 0.05$ and $\varepsilon = 0.02$. The profiles of vector $\mathbf{u}$ and images of pressure p at different time slots $t = 5, 20, 100, 300$ are presented. (For interpretation of the colors in the figure(s), the reader is referred to the web version of this article.)

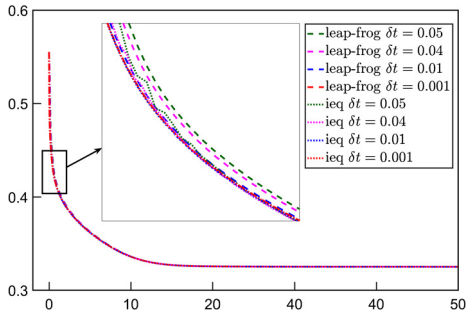

Fig. 3.6. Time evolution of the energy for the CHNS model when $t \in [0, 50]$ with $\eta = 0.1$, $M = 0.1$, $\gamma = 0.05$ and $\varepsilon = 0.05$.

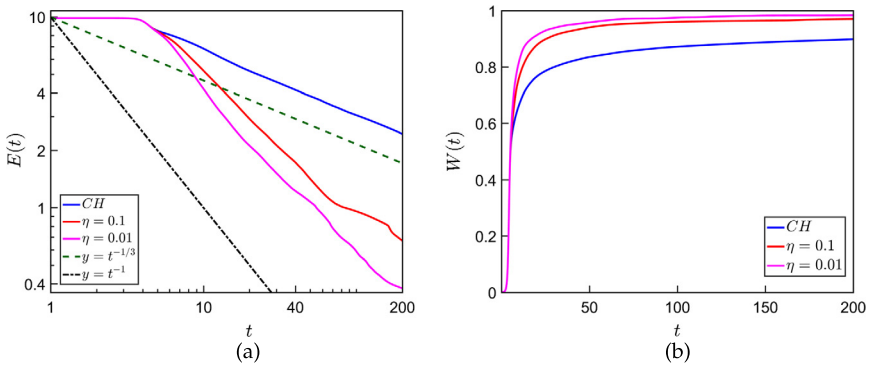

Fig. 3.7. Time evolution of the energy (a) and roughness (b) for the CH model and CHNS model using with a random initial condition for $t \in [1, 200]$ and $t \in [0, 200]$ respectively.

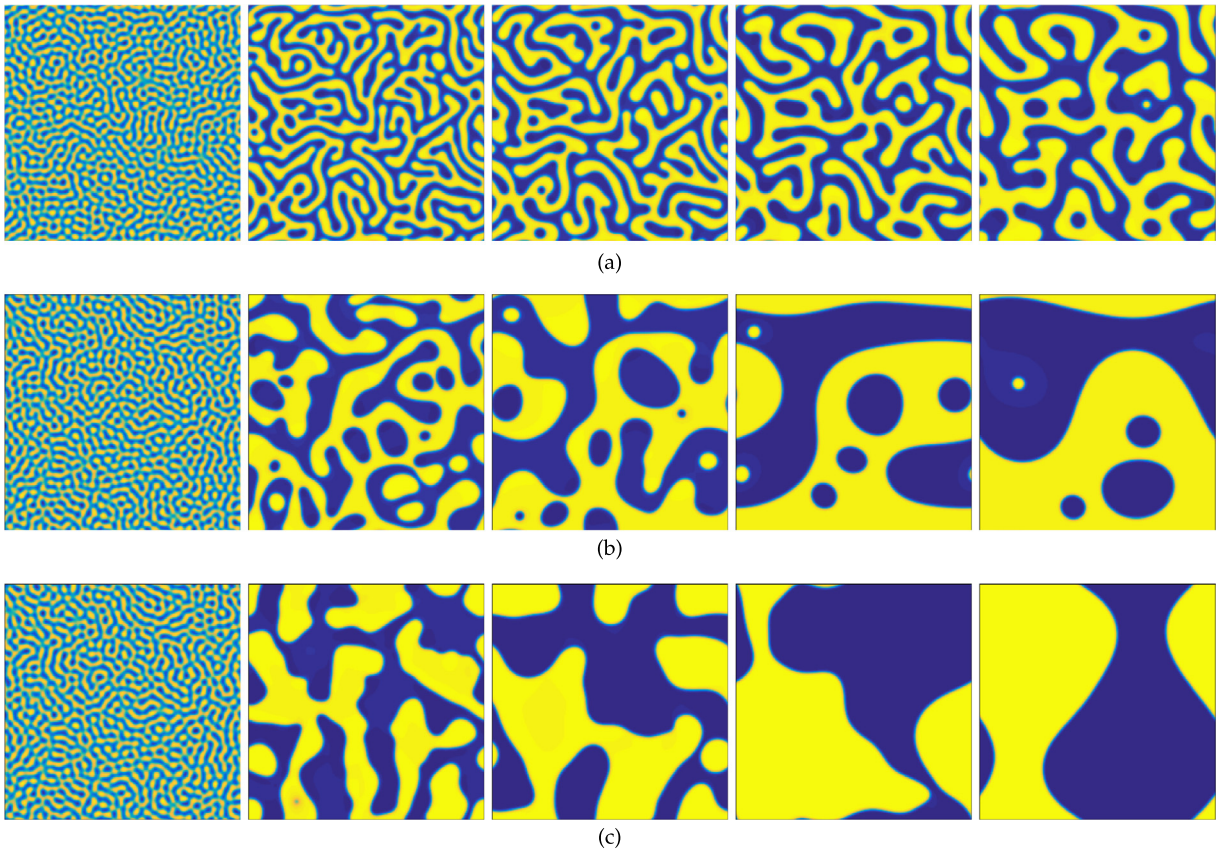

Fig. 3.8. Time snapshots of coarsening dynamics (a) driven by the CH model with $\gamma = 0.02$ and $\varepsilon = 0.05$; (b) driven by the CHNS model with $M = 0.02$, $\gamma = 0.05$, $\varepsilon = 0.05$ and $\eta = 0.1$; (c) driven by the CHNS model with $M = 0.02$, $\gamma = 0.05$, $\varepsilon = 0.05$ and $\eta = 0.01$. Snapshots are taken at $t = 5, 25, 50, 100, 200$.

phase variables, in this example. In Fig. 3.9, we present the profiles of vector **u** and color plots of pressure p at different times. It is observed that the velocity field of the CHNS model has a larger effect on the interface than in bulk, as we see larger velocity magnitude at the interface. And, we also observe larger pressure gradients at the phase interface.

3.4. Nucleation dynamics

In this following example, we consider the nucleation dynamics with the CHNS system. We consider the computational domain $[0, 2\pi] \times [0, 2\pi]$ and use the following initial profile

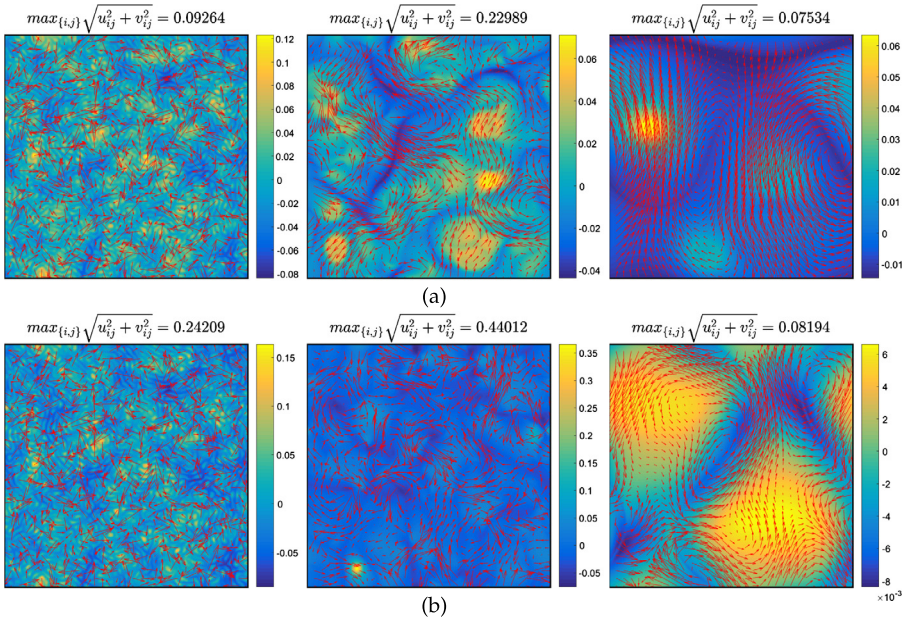

Fig. 3.9. Time snapshots of coarsening dynamics driven by the CHNS model. In this figure, (a) shows the profiles of $\mathbf{u}$ with parameters $\eta = 0.1$, $M = 0.02$, $\gamma = 0.05$ and $\varepsilon = 0.05$; (b) shows the profiles of $\mathbf{u}$ with parameters $\eta = 0.01$, $M = 0.02$, $\gamma = 0.05$ and $\varepsilon = 0.05$. Snapshots are taken at $t = 5, 25, 200$.

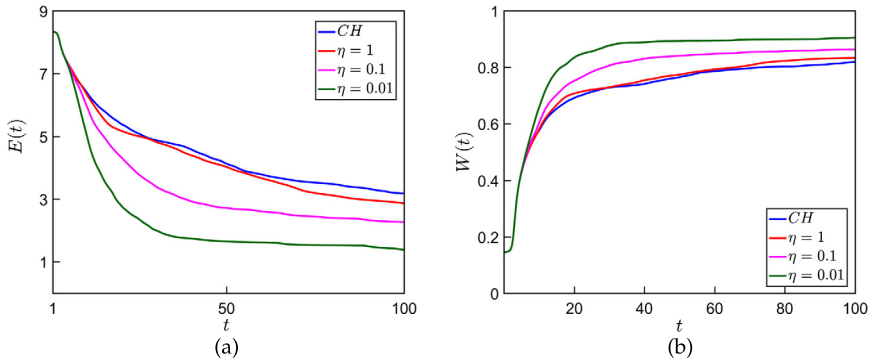

Fig. 3.10. Time evolution of the energy (a) and the roughness (b) for the CH model and the CHNS model using with a random initial condition. In this figure, the evolution of the energy for $t \in [1, 100]$ and the roughness for $t \in [0, 100]$ are summarized.

$$\begin{cases} \mathbf{u}^0(x, y) = \mathbf{0}, \forall (x, y) \in \Omega, \\ \phi^0(x, y) = \dfrac{|x - \pi|}{2\pi} + 10^{-3} \times rand(-1, 1), \quad \forall (x, y) \in \Omega. \end{cases} \tag{3.5}$$

Notice with this initial profile $\phi^0(x, y)$ for the phase variable, the averaged volume fraction of ϕ varies spatially, with a larger value near the sides, and smaller values in the middle. Also, we fix the physical parameters $M = 0.02,\ \gamma = 0.05,\ \varepsilon = 0.05$ and computational parameters $\delta t = 0.001, N = 256$.

As a comparison, we solve the CHNS system with various viscosity parameters, as well as the CH equation alone. The time evolution of the energy and roughness are summarized in Fig. 3.10. We observe that the hydrodynamics will facilitate the nucleation dynamics and speed up the energy decay dramatically.

Then, in Fig. 3.11, we plot the contour lines of numerical solutions of the phase function ϕ for the CH model and CHNS with $\eta = 1, 0.1, 0.01$, respectively. Snapshots are taken at $t = 1, 5, 10, 20, 100$, respectively. In this example, we observe both spinodal decomposition and nucleation are taking place on different parts of the computational domain, similarly as [20]. And in particular, the spinodal decomposition takes place where there are bigger averaged volume fractions, and the nucleation takes place, where there are smaller, averaged volume fraction. For the CH model, the band structure in the middle is preserved, while for the CHNS model with smaller viscosity, the band structure is broken, and a circular drop is formed, instead. In addition, we observe that the hydrodynamics has a tremendous influence on the phase evolution as the above example. And, when the fluid has a smaller viscosity, the effect is more obvious.

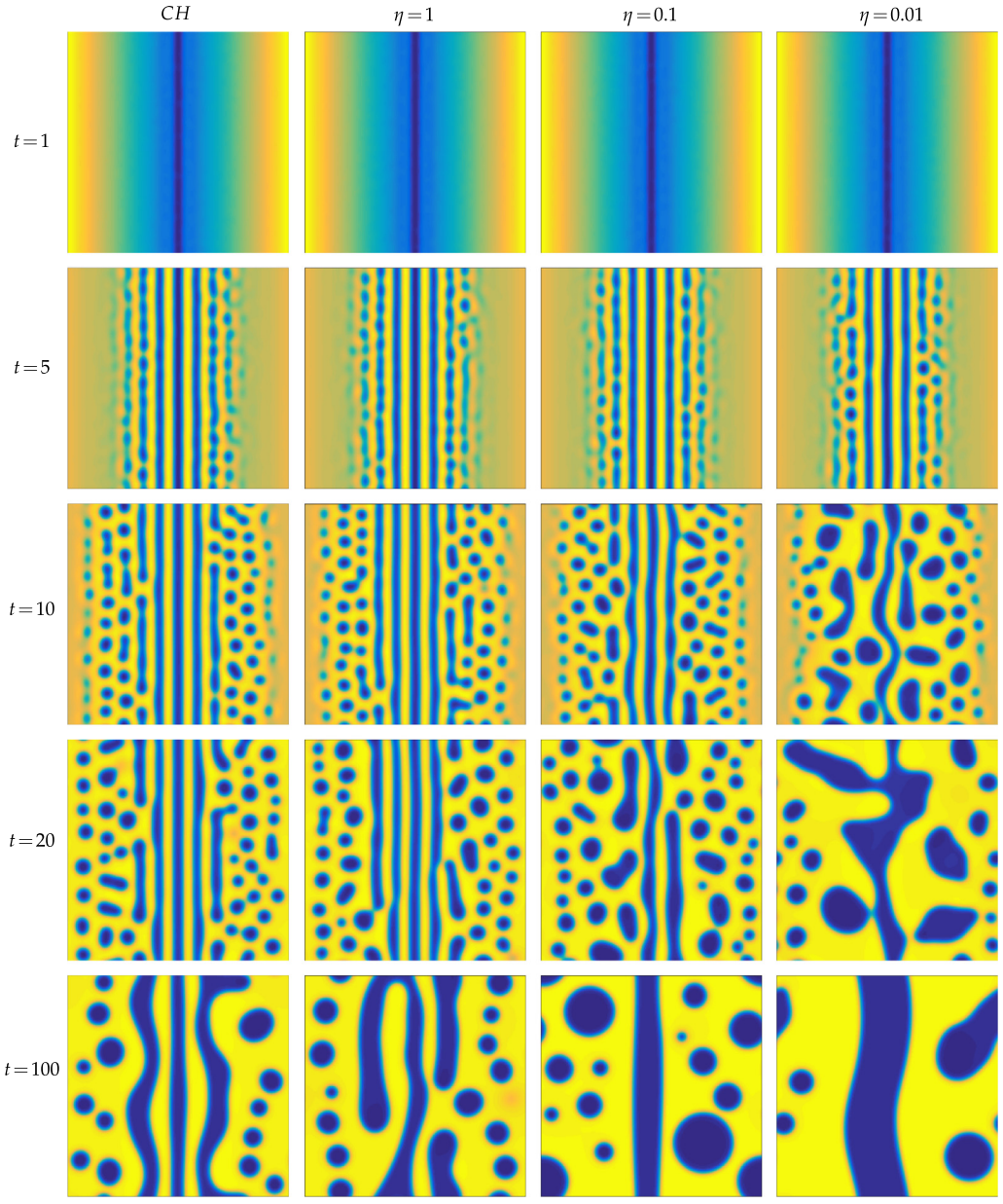

Fig. 3.11. Time snapshots of phase separation dynamics driven by the CH model and the CHNS model with various viscosities, here we fix $M = 0.02$, $\gamma = 0.05$ and $\varepsilon = 0.05$. The profiles of ϕ at different time slots $t = 1, 5, 10, 20, 100$ are presented.

Finally, we plot the profiles of the velocity $\mathbf{u}$ by vector fields and the pressure p by a color field at $t = 1, 5, 10, 100$ in Fig. 3.12. Similarly, as the previous two examples, large velocity fields locate on the interface, which drive the phase evolution. And we observe that the pressure has a larger gradient at the interface in all cases, which also agrees with the previous two examples. In particular, we observe the case with a smaller viscosity evolves faster than the case with a larger viscosity.

4. Conclusion

In this paper, by utilizing the modified leap-frog finite difference method for temporal discretization and Fourier pseudospectral method for spatial discretization, we come up with a novel numerical algorithm for solving the Cahn-Hilliard-Navier-Stokes (CHNS) equation. The newly proposed algorithm is second-order accurate in time and spectral accurate in space. Also, it is linear, such that only a linear algebraic system needed to be solved in each time step. And the numerical scheme is proved to be unconditionally energy stable, which is also further verified numerically through several examples

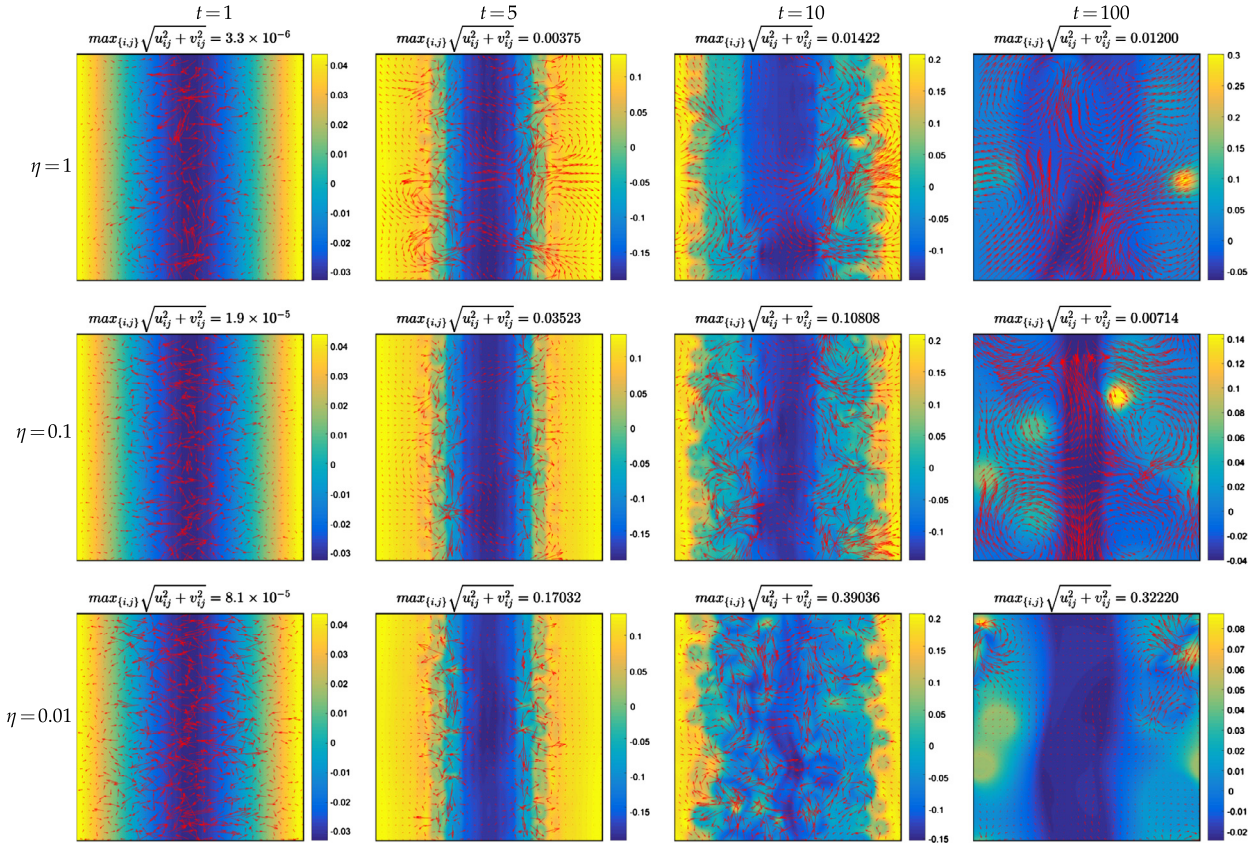

Fig. 3.12. Time snapshots of phase separation dynamics driven by the CHNS model with different viscosities. Here we fix the parameters $M = 0.02$, $\gamma = 0.05$ and $\varepsilon = 0.05$. The profiles of vector field $\mathbf{u}$ and color plots of pressure p at different time slots $t = 1, 5, 10, 100$ are presented.

of coarsening and phase separation dynamics. In addition, we solve the CHNS system for several cases with various physical parameters, confirming the effectiveness of the newly proposed scheme. Furthermore, the proposed numerical techniques in this paper could be easily applied to investigate other phase-field hydrodynamics models for multiphase fluids, quasi-incompressible fluids, and complex fluids.

Data availability statement

The datasets generated during and/or analyzed during the current study are available from the corresponding author on reasonable request.

CRediT authorship contribution statement

Lizhen Chen: Data curation, Formal analysis, Software, Validation, Visualization, Writing - original draft. **Jia Zhao:** Conceptualization, Formal analysis, Methodology, Writing - original draft.

Declaration of competing interest

The authors declare that they have no known competing financial interests or personal relationships that could have appeared to influence the work reported in this paper.

Acknowledgements

Lizhen Chen would like to acknowledge the support from the National Natural Science Foundation of China Grants 11671166 and U1930402. Jia Zhao would like to acknowledge the support from National Science Foundation with grant NSF-DMS-1816783.

References

[1] H. Abels, H. Garcke, G. Grün, Thermodynamically consistent, frame indifferent diffuse interface models for incompressible two-phase flows with different densities, Math. Models Methods Appl. Sci. 22 (03) (2012) 1150013.
[2] J. Bosch, C. Kahle, M. Stoll, Preconditioning of a coupled Cahn-Hilliard Navier-Stokes system, Commun. Comput. Phys. 23 (2018) 603–628.
[3] F. Boyer, C. Lapuerta, S. Minjeaud, B. Piar, M. Quintard, Cahn-Hilliard/Navier-Stokes model for the simulation of three-phase flows, Transp. Porous Media 82 (2010) 463–483.
[4] Y. Brenier, F. Otto, C. Seis, Upper bounds on coarsening rates in demixing binary viscous liquids, SIAM J. Math. Anal. 43 (1) (2011) 114–134.
[5] Y. Cai, H. Choi, J. Shen, Error estimates for time discretizations of Cahn-Hilliard and Allen-Cahn phase-field models for two-phase incompressible flows, Numer. Math. 137 (2017) 417–449.
[6] Y. Cai, J. Shen, Error estimates for a fully discretized scheme to a Cahn-Hilliard phase-field models for two-phase incompressible flows, Math. Comput. 87 (313) (2018).
[7] L. Chen, J. Zhao, Y. Gong, A novel second-order scheme for the molecular beam epitaxy model with slope selection, Commun. Comput. Phys. 25 (4) (2019) 1024–1044.
[8] L. Chen, J. Zhao, X. Yang, Regularized linear schemes for the molecular beam epitaxy model with slope selection, Appl. Numer. Math. 128 (2018) 138–156.
[9] W. Chen, W. Feng, Y. Liu, C. Wang, S. Wise, A second order energy stable scheme for the Cahn-Hilliard-Hele-Shaw equations, Discrete Contin. Dyn. Syst., Ser. B 24 (1531) (2016) 149.
[10] W. Chen, Y. Liu, C. Wang, S. Wise, Convergence analysis of a fully discrete finite difference scheme for Cahn-Hilliard-Hele-Shaw equation, Math. Comput. 85 (301) (2016) 2231–2257.
[11] Y. Chen, J. Shen, Efficient adaptive energy stable schemes for the incompressible Cahn-Hilliard Navier-Stokes phase-field models, J. Comput. Phys. 308 (2016) 40–56.
[12] K. Cheng, W. Feng, C. Wang, S. Wise, An energy stable fourth order finite difference scheme for the Cahn-Hilliard equation, J. Comput. Appl. Math. 362 (574–595) (2019).
[13] K. Cheng, C. Wang, S. Wise, X. Yue, A second-order weakly energy-stable pseudo-spectral scheme for the Cahn-Hilliard equation and its solution by the homogeneous linear iteration method, J. Sci. Comput. 69 (3) (2016) 1083–1114.
[14] A. Diegel, X. Feng, S. Wise, Analysis of a mixed finite element method for a Cahn-Hilliard-Darcy-Stokes system, SIAM J. Numer. Anal. 53 (1) (2015) 127–152.
[15] A. Diegel, C. Wang, X. Wang, S. Wise, Convergence analysis and error estimates for a second order accurate finite element method for the Cahn-Hilliard-Navier-Stokes system, Numer. Math. 137 (2017) 495–534.
[16] A. Diegel, C. Wang, S. Wise, Stability and convergence of a second-order mixed finite element method for the Cahn-Hilliard equation, IMA J. Numer. Anal. 36 (2016) 1867–1897.
[17] S. Dong, J. Shen, A time stepping scheme involving constant coefficient matrices for phase field simulations of two phase incompressible flows with large density ratios, J. Comput. Phys. 231 (2012) 5788–5804.
[18] D. Eyre, Unconditionally gradient stable time marching the Cahn-Hilliard equation, Mat. Res. Soc. Symp. Proc. 529 (1998) 39–46.
[19] X. Feng, Fully discrete finite element approximations of the Navier-Stokes-Cahn-Hilliard diffuse interface model for two-phase fluid flows, SIAM J. Numer. Anal. 44 (3) (2006) 1049–1072.
[20] H. Gomez, T.J.R. Hughes, Provably unconditionally stable, second-order time-accurate, mixed variational methods for phase-field models, J. Comput. Phys. 230 (13) (2011) 5310–5327.
[21] Y. Gong, J. Zhao, Energy-stable Runge-Kutta schemes for gradient flow models using the energy quadratization approach, Appl. Math. Lett. 94 (2019) 224–231.
[22] Y. Gong, J. Zhao, Q. Wang, An energy stable algorithm for a quasi-incompressible hydrodynamic phase-field model of viscous fluid mixtures with variable densities and viscosities, Comput. Phys. Commun. 219 (2017) 20–34.
[23] Y. Gong, J. Zhao, Q. Wang, Linear second order in time energy stable schemes for hydrodynamic models of binary mixtures based on a spatially pseudospectral approximation, Adv. Comput. Math. 44 (2018) 1573–1600.
[24] Y. Gong, J. Zhao, Q. Wang, Second order fully discrete energy stable methods on staggered grids for hydrodynamic phase field models of binary viscous fluids, SIAM J. Sci. Comput. 40 (2) (2018) B528–B553.
[25] Y. Gong, J. Zhao, X. Yang, Q. Wang, Second-order linear schemes for hydrodynamic phase field models of viscous fluid flows with variable densities, SIAM J. Sci. Comput. 4 (1) (2018) B138–B167.
[26] B.E. Griffith, An accurate and efficient method for the incompressible Navier-Stokes equations using the projection method as a preconditioner, J. Comput. Phys. 228 (20) (2009) 7565–7595.
[27] G. Grün, F. Klingbeil, Two-phase flow with mass density contrast: stable schemes for a thermodynamic consistent and frame-indifferent diffuse-interface model, J. Comput. Phys. 257 (2014) 708–725.
[28] F. Guillén-González, G. Tierra, On linear schemes for a Cahn-Hilliard diffuse interface model, J. Comput. Phys. 234 (2013) 140–171.
[29] F. Guillén-González, G. Tierra, Second order schemes and time-step adaptivity for Allen-Cahn and Cahn-Hilliard models, Comput. Math. Appl. 68 (2014) 821–846.
[30] F. Guillén-González, G. Tierra, Splitting schemes for a Navier-Stokes-Cahn-Hilliard model for two fluids with different densities, J. Comput. Math. 32 (6) (2014) 643–664.
[31] J. Guo, C. Wang, S. Wise, X. Yue, An H^2 convergence of a second-order convex-splitting, finite difference scheme for the three-dimensional Cahn-Hilliard equation, Commun. Math. Sci. 14 (2) (2015) 489–515.
[32] Z. Guo, P. Lin, A thermodynamically consistent phase-field model for two-phase flows with thermocapillary effects, J. Fluid Mech. 766 (2015) 226–271.
[33] Z. Guo, P. Lin, J. Lowengrub, A numerical method for the quasi-incompressible Cahn-Hilliard-Navier-Stokes equations for variable density flows with a discrete energy law, J. Comput. Phys. 276 (2014) 486–507.
[34] Z. Guo, P. Lin, J. Lowengrub, S. Wise, Mass conservative and energy stable finite difference methods for the quasi-incompressible Navier-Stokes-Cahn-Hilliard system: primitive variable and projection-type schemes, Comput. Methods Appl. Mech. Eng. 326 (2017) 144–174.
[35] D. Han, N. Jiang, A second order, linear, unconditionally stable, Crank-Nicolson-Leapfrog scheme for phase field models of two-phase incompressible flows, Appl. Math. Lett. 108 (2020) 106521.
[36] D. Han, X. Wang, A second order in time uniquely solvable unconditionally stable numerical schemes for Cahn-Hilliard-Navier-Stokes equation, J. Comput. Phys. 290 (1) (2015) 139–156.
[37] Y. Liu, W. Chen, C. Wang, S. Wise, Error analysis of a mixed finite element method for a Cahn-Hilliard-Hele-Shaw system, Numer. Math. 135 (3) (2017) 679–709.
[38] J.S. Lowengrub, L. Truskinovsky, Quasi incompressible Cahn-Hilliard fluids and topological transitions, Proc. R. Soc. A, Math. Phys. Eng. Sci. 454 (1998) 2617–2654.
[39] S. Minjeaud, An unconditionally stable uncoupled scheme for a triphasic Cahn-Hilliard/Navier-Stokes model, Numer. Methods Partial Differ. Equ. 29 (2) (2013) 584–618.

[40] Z. Qiao, Z. Zhang, T. Tang, An adaptive time-stepping strategy for the molecular beam epitaxy models, SIAM J. Sci. Comput. 33 (3) (2011) 1395–1414.
[41] J. Shen, J. Xu, J. Yang, The scalar auxiliary variable (SAV) approach for gradient flows, J. Comput. Phys. 353 (2018) 407–416.
[42] J. Shen, X. Yang, Decoupled energy stable schemes for phase field models of two phase incompressible flows, SIAM J. Numer. Anal. 53 (1) (2015) 279–296.
[43] C. Wang, X. Wang, S. Wise, Unconditionally stable schemes for equations of thin film epitaxy, Discrete Contin. Dyn. Syst. 28 (1) (2010) 405–423.
[44] C. Wang, S. Wise, An energy stable and convergent finite-difference scheme for the modified phase field crystal equation, SIAM J. Numer. Anal. 49 (3) (2011) 945–969.
[45] Y. Yan, W. Chen, C. Wang, S. Wise, A second-order energy stable BDF numerical scheme for the Cahn-Hilliard equation, Commun. Comput. Phys. 23 (2) (2018) 572–602.
[46] X. Yang, J. Zhao, Q. Wang, Numerical approximations for the molecular beam epitaxial growth model based on the invariant energy quadratization method, J. Comput. Phys. 333 (2017) 102–127.
[47] X. Yang, J. Zhao, Q. Wang, J. Shen, Numerical approximations for a three components Cahn-Hilliard phase-field model based on the invariant energy quadratization method, Math. Models Methods Appl. Sci. 27 (2017) 1993–2023.
[48] J. Zhao, H. Li, Q. Wang, X. Yang, A linearly decoupled energy stable scheme for phase-field models of three-phase incompressible flows, J. Sci. Comput. 70 (2017) 1367–1389.
[49] J. Zhao, X. Yang, Y. Gong, X. Zhao, X. Yang, J. Li, Q. Wang, A general strategy for numerical approximations of non-equilibrium models–Part I: Thermodynamical systems, Int. J. Numer. Anal. Model. 15 (6) (2018) 884–918.